ELSEVIER

Journal of Nuclear Materials 244 (1997) 295–304

journal of nuclear materials

The formation of bubbles in Zr alloys under Kr ion irradiation

L. Pagano Jr. [a], A.T. Motta [a,*], R.C. Birtcher [b]

[a] *Department of Nuclear Engineering, The Pennsylvania State University, University Park, PA 16802-1408, USA*
[b] *Materials Science Division, Argonne National Laboratory, Argonne, IL 60439, USA*

Received 24 May 1996; accepted 26 November 1996

Abstract

We report here a study of Kr ion implantation and resultant bubble formation in Zr and Zr alloys, including Zircaloy-2 and Zircaloy-4. Implantations into thin foils were performed in-situ in the HVEM/Tandem facility at Argonne National Laboratory at temperatures between 300 to 800°C and to doses up to 2×10^{20} ion m^{-2}. Bulk specimens were implanted in an ion-beam chamber and then thinned for viewing by TEM. In thin foils, only small bubbles (3–10 nm) were formed at all temperatures with the exception of the Cr-rich Valloy where 13 nm bubbles were formed. Bulk samples implanted at 300°C contained a bubble morphology similar to that observed after implantation into thin foils. However at high temperatures (500–800°C) large faceted bubbles (up to 30 nm) were produced in bulk specimens. The results indicate that bubble formation and evolution below 500°C is controlled by gas concentration, while it is controlled by bubble mobility at high temperatures.

1. Introduction

In addition to their low neutron absorption cross section and excellent high temperature corrosion resistance, one of the properties of Zr alloys that has made them very attractive for use in nuclear power applications is their remarkable resistance to void swelling during in-reactor neutron irradiation [1]. In contrast to other metals and to other alloys used for nuclear fuel cladding, such as stainless steel, Zr and Zr alloys exhibit little void formation and, as a consequence, little swelling when exposed to irradiation.

Throughout this work we use the term 'void' to refer to a three-dimensional aggregation of vacancies, the term 'bubble' for a void containing gas, and 'cavity' as a generic term encompassing both. The few examples of radiation-induced cavities in Zr alloys have generally involved the irradiation of samples pre-implanted with insoluble noble gases such as He and Ne [2,3]. Zirconium is peculiar in that both vacancy *and* interstitial loops are stable under irradiation (usually one type grows at the expense of the other). When only interstitial loops are present voids can grow by absorbing excess vacancies. The vacancy loops represent an alternative route to voids for the evolution of small vacancy clusters. The insoluble gases negate this route, by stabilizing small void embryos against collapse to vacancy loops [4]. The anisotropic nature of Zr also causes it to behave differently from cubic materials under irradiation. In particular, the defect migration energies in the $\langle c \rangle$ and $\langle a \rangle$ directions are different. This migration anisotropy is linked to the presence of trace Fe in the Zr matrix [5].

The formation of voids under irradiation has been observed in a large number of metals and alloys [6]. Void formation is made possible by the establishment of a high supersaturation of point defects under irradiation. The constant production and annihilation of defects, especially vacancies, can promote the nucleation and growth of voids and bubbles. For voids to grow in metals during irradiation they must receive a net flux of vacancies to voids. This means that interstitials (produced in equal numbers by irradiation), must be preferentially absorbed in other sinks in the microstructure of the material.

Extensive evidence of void formation in metals has accumulated over the past decades [6,7]. Notably, a few elements (Zr, Ti) have shown a remarkable resistance to

* Corresponding author.

PII S0022-3115(96)00757-X

Table 1
Chemical composition (wt%) of the studied materials

Alloy	Sn	Fe	Cr	Ni	Nb
Zircaloy-4	1.5	0.21	0.1	[a]	[a]
Zircaloy-2	1.6	0.15	0.1	0.05	[a]
NSF	1.0	0.2	[a]	0.05	0.6
Valloy	[a]	0.1	1.1	[a]	[a]
Zr–NP	impurities less than 0.2 wt%				

[a] Traces. Other minor constituents not reported as well.

void formation [8]. Studies have been performed of void formation in Zr and Zr alloys under both neutron [9–11] and charged particle irradiation [12–14]. Examination of neutron-irradiated Zircaloy has occasionally revealed cavities especially after high fluences, when, presumably, enough He has been produced by (n, α) reactions. Gilbert et al. [9] identified the few cavities they observed in Zircaloy after neutron irradiation to 10^{25} n m^{-2} ($E > 0.1$ MeV) as equilibrium gas bubbles. The work of Buckley and Manthorpe [12] showed that voids are formed in zirconium during electron irradiation, and the maximum swelling occurs at 450–500°C. They also found that voids grew more readily in samples that had been previously doped with 10^{-5} Xe than in undoped samples. However their experiments were influenced by bad vacuum conditions in the microscope during irradiation. Jostsons et al. [10] found voids in pure Zr neutron-irradiated to 1.3×10^{25} n m^{-2} only in the temperature range 400 to 500°C, and only in the samples that had the highest B content (1 appm). Faulkner and Woo [13] studied void swelling in zirconium under electron irradiation and found that the pre-injection of He was essential for void development. Specimens implanted with 100 ppm He developed voids while those implanted with 10 ppm or less did not. Their maximum swelling temperature of 450°C agrees well with the results from Jostsons et al. and Buckley and Manthorpe. Finally it has recently been demonstrated that electron irradiation to 50–70 dpa at 500°C creates cavities in Zircaloy previously irradiated with neutrons (0.2×10^{25} n m^{-2}) [14].

The study of cavity formation in other metals has advanced considerably in recent years [15]. Implantation of noble gases into metals such as Al [16,17], Ni [18,19], Ti [20] and Mo [21] results in the formation of solid noble gas precipitates. These solid precipitates form inside very high pressure bubbles. As the bubble or solid precipitate grows the precipitate melts and the bubbles become mobile leading to coalescence and rapid bubble growth. During Kr implantation of Ni, Birtcher and Liu [18] observed that as the temperature increased, a bimodal bubble distribution appeared, which coincided with the disappearance of the solid Kr diffraction spots. Other studies have shown void lattice formation in different metals [22].

Such systematic studies have not been performed for Zr. We have in this work conducted a systematic study of the conditions of bubble formation in zirconium alloys under Kr ion irradiation. The objective was to determine the temperature regime and irradiation conditions where large bubbles are formed, either by bubble mobility and coalescence, or by aggregation of vacancies and gas atoms. A second goal was to derive mechanistic understanding of the process of bubble formation and growth in zirconium alloys during implantation.

2. Experimental methods

This work consisted of two distinct types of specimens denoted 'thin foil' and 'bulk' that were used for either in-situ or ex-situ implantations. The implantations were performed in the HVEM/Tandem User Facility at Argonne National Laboratory (ANL) using a 650 keV NEC ion implanter. Implantations were done either 'in-situ' with the sample placed in a TEM specimen holder in the

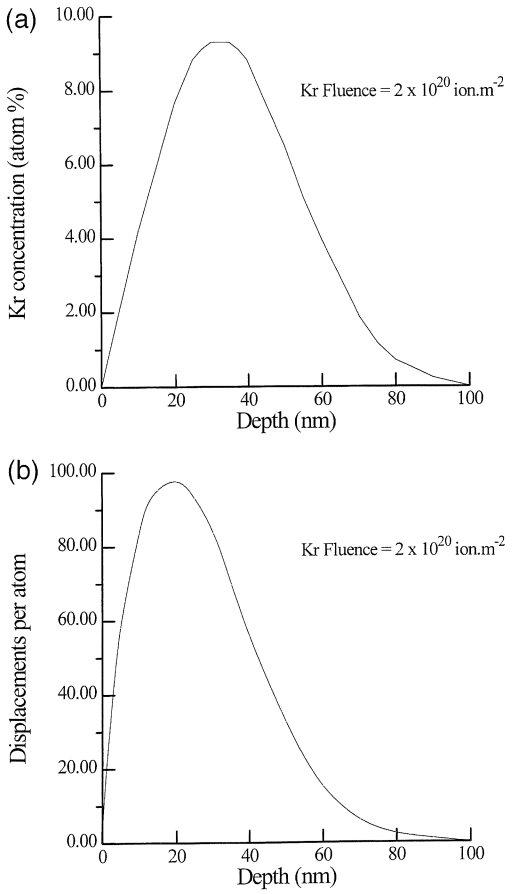

Fig. 1. (a) Concentration profile of implanted Kr atoms and (b) displacement profile in Zr, after 100 keV Kr irradiation to 2×10^{20} ion m^{-2} as calculated by TRIM [24].

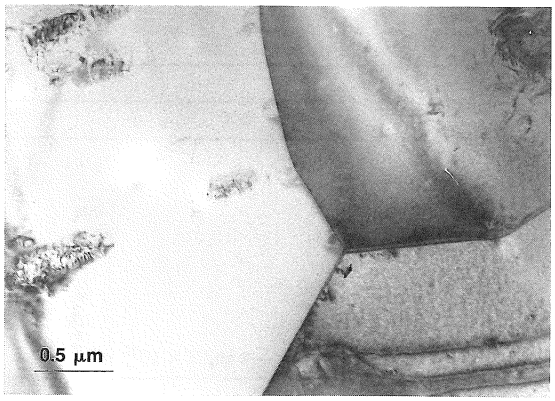

Fig. 2. Bright field TEM micrograph of recrystallized Zircaloy-4 before irradiation.

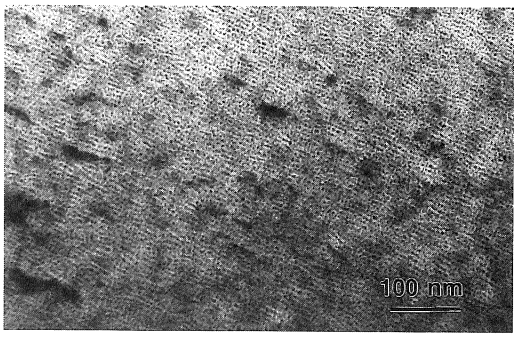

Fig. 4. Bright field contrast in overfocus condition of bubble morphology in nominally pure Zr, after irradiation with 100 keV Kr ions to 2×10^{20} ion m^{-2} at 500°C, under thin foil conditions. Only small bubbles, 3–5 nm, are seen, with some evidence of bubble alignment.

High Voltage Electron Microscope, or in an ion-beam specimen chamber. The vacuum in the HVEM and in the accelerator target line was $1-2\times10^{-7}$ Torr. Samples were examined before and after irradiation in the Phillips EM420 in the Materials Characterization Laboratory (MCL) at Pennsylvania State University (PSU), and on the JEOL 100CX at ANL.

Zr alloys were furnished by General Electric Corporation. Their composition is shown in Table 1. For the 'thin foil' experiments, 3 mm diameter, 0.1 mm thickness disks were prepared by cutting and mechanical polishing. Trans-

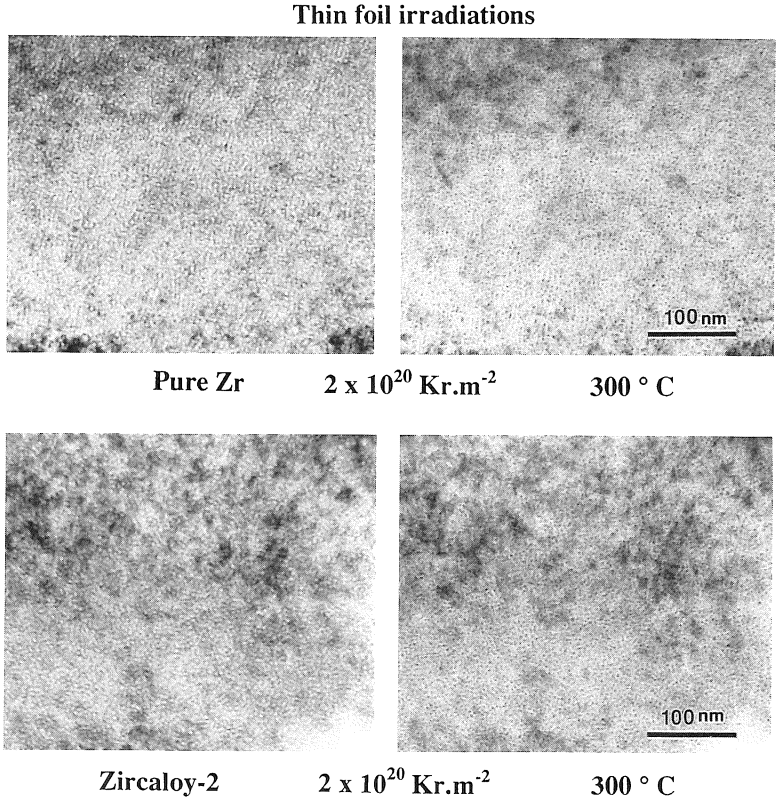

Fig. 3. Bright field contrast in underfocus and overfocus conditions of bubble morphology in thin foil of nominally pure Zr and Zircaloy-2 after irradiation with 100 keV Kr ions to 2×10^{20} ion m^{-2} at 300°C. Only small bubbles, 3–4 nm diameter, are seen.

Table 2
Irradiation experiments conducted

	T (°C)			
	300	500	700	800
Thin foil irradiation				
Zircaloy-4	2×10^{20} m^{-2}	2×10^{20} m^{-2}	2×10^{20} m^{-2}	
Zircaloy-2	2×10^{20} m^{-2}	2×10^{20} m^{-2}	2×10^{20} m^{-2}	
Zirconium	2×10^{20} m^{-2}	2×10^{20} m^{-2}		
Valloy	2×10^{20} m^{-2}	2×10^{20} m^{-2}	2×10^{20} m^{-2}	
NSF	2×10^{20} m^{-2}	2×10^{20} m^{-2}		
Bulk sample irradiation				
Zircaloy-4	1 and 2×10^{20} m^{-2}	1 and 2×10^{20} m^{-2}	1 and 2×10^{20} m^{-2}	1 and 2×10^{20} m^{-2}

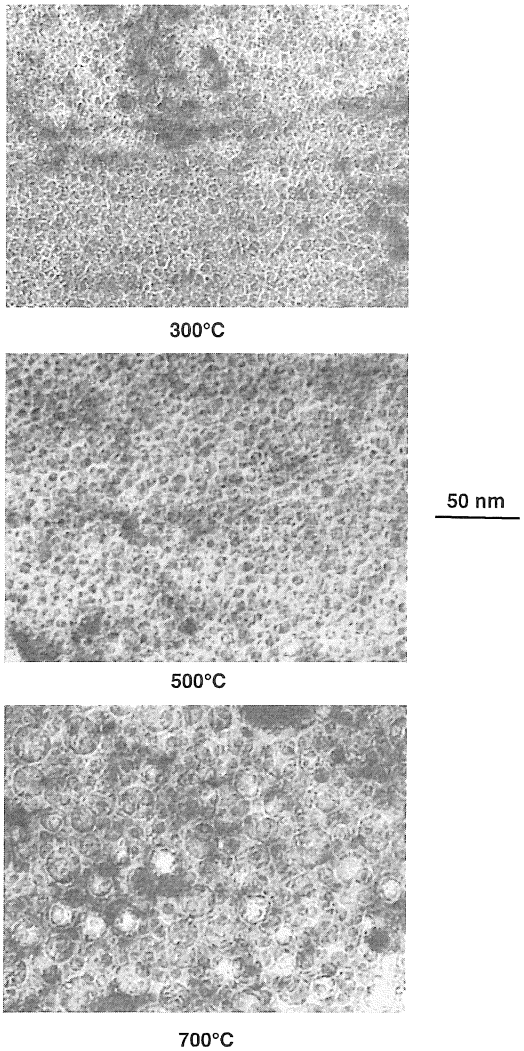

Fig. 5. Bright field micrographs of Zircaloy-4 irradiated with 100 keV Kr ions in bulk geometry to 2×10^{20} ion m^{-2}, at three different temperatures: (a) 300°C, (b) 500°C, (c) 700°C.

mission electron microscopy (TEM) samples were made by electropolishing in a solution of 10% perchloric acid in methanol, kept at −40°C, or in a solution of 5.3 g LiCl, 11.16 g $Mg(ClO_4)_2$, 500 ml methanol and 100 ml butyl–cellusolve kept at −50°C [23].

These samples were then irradiated with 100 keV Kr ions to fluences up to 2×10^{20} ion m^{-2}. The Kr ion distribution and displacement rate in Zr as calculated by TRIM [24], is shown in Fig. 1. The peak in the ion concentration occurs at a depth of 36 nm while the displacement peak occurs at 20 nm. The width of the concen-

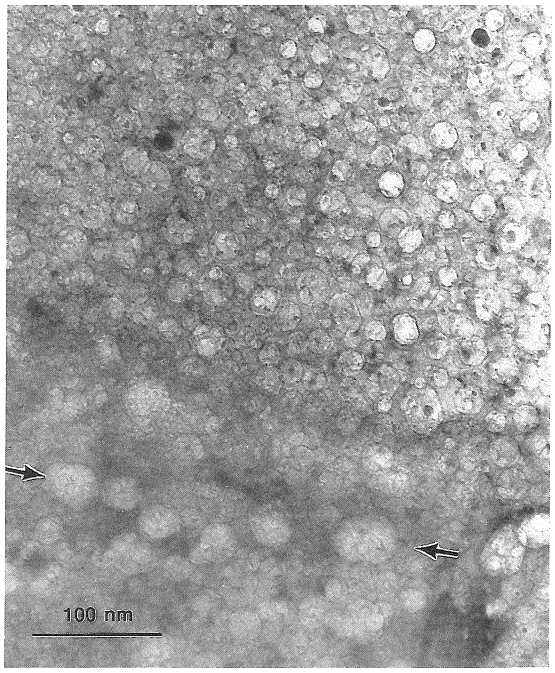

Fig. 6. Bright field micrograph showing large bubbles at grain boundaries in bulk Zircaloy-4 irradiated with 100 keV Kr ions at 700°C to 2×10^{20} ion m^{-2}.

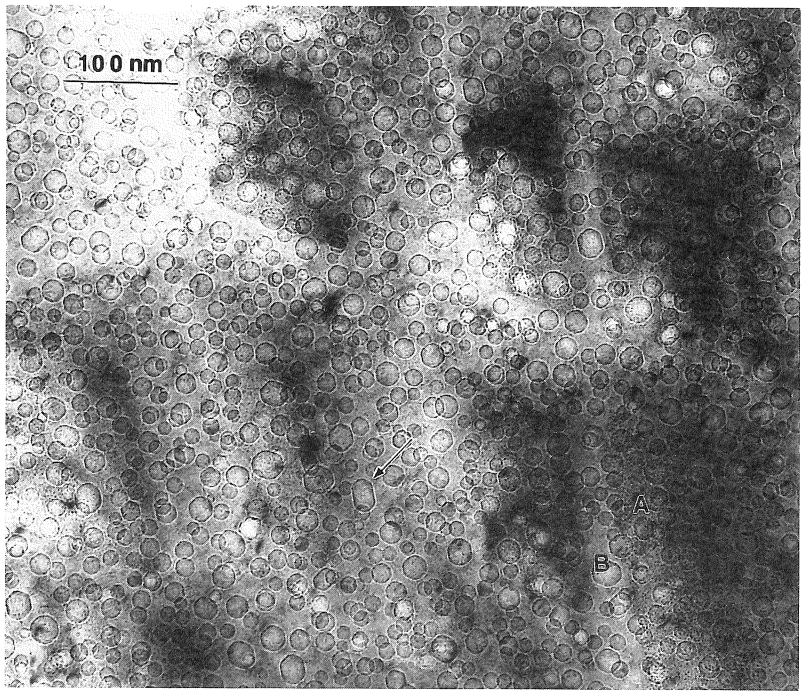

Fig. 7. Bright field micrograph of bulk Zircaloy-4 irradiated with 100 keV Kr ions to 2×10^{20} ion m^{-2}, at 800°C. Large faceted bubbles are seen throughout the specimen. Bubble coalescence is also observed (arrowed). The precipitates seen in Fig. 8 are out of contrast, but their outline can be barely discerned. A higher density of small bubbles is seen within the precipitate outline ('A') rather than in-between ('B').

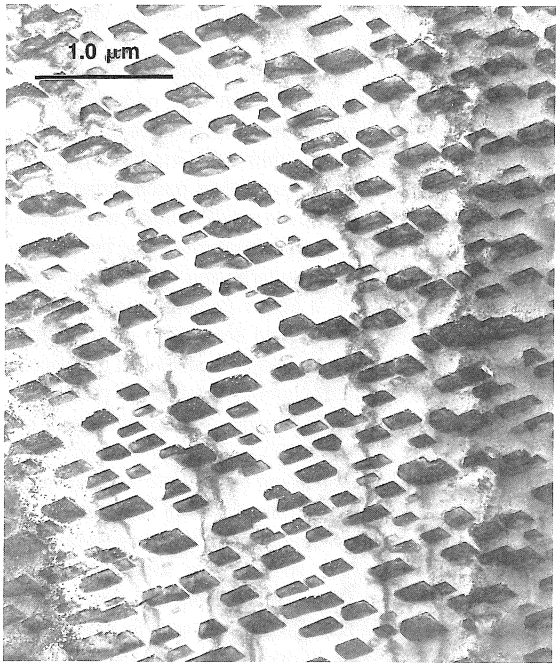

Fig. 8. Bright field contrast of unidentified plate-like precipitates formed in bulk Zircaloy-4 after irradiation with 100 keV Kr ions to 2×10^{20} ion m^{-2}, at 800°C.

tration peak is narrow enough that most of the gas is deposited within a 100 nm foil. The level of damage calculated by TRIM at the half maximum of the Bragg peak was 1 dpa per 4.4×10^{18} ion m^{-2}, using $E_d = 25$ eV. The peak damage level at 2×10^{20} ion m^{-2} corresponds thus to 45 dpa. The Kr concentration in the 1 nm region around the peak is 9 at%. The bulk irradiations were conducted in the same fashion, except that the samples were thinned after implantation by covering the implanted face with lacquer and thinning from the other side.

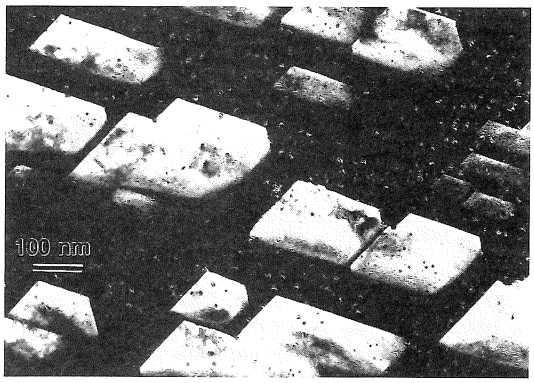

Fig. 9. Dark field contrast of unidentified precipitates in Fig. 8.

A bright field TEM micrograph of the microstructure of Zircaloy-4 is shown in Fig. 2; a fully recrystallized structure was obtained, with large equiaxed grains, and low dislocation density. No damage from the mechanical polishing was detected. The samples pre-thinned before irradiation had an overall thickness of 100–150 nm in the electron thin areas, while the bulk samples had a thickness of 1 mm. Although in the bulk samples the implantation is also done within 35 nm of the free surface, there is only one free surface close to the irradiated area, as compared to two in the thin foil case. This difference is important, as will be seen below.

Irradiations of Zircaloy-4 were made for all the irradiation conditions used (bulk and thin foil implanting, temperatures from 300–800°C, and fluences of $1–2 \times 10^{20}$ ion m^{-2}), and all the alloys in Table 1 for thin foil irradiation at 300–700°C to 2×10^{20} ion m^{-2}. A summary of the irradiation experiments conducted is shown in Table 2.

3. Results

Fig. 3 shows overfocus/underfocus pairs taken from thin foil Zircaloy-2 and nominal purity zirconium specimens after irradiation at a temperatures of 300°C to a dose of 2×10^{20} ion m^{-2}. An even distribution of small bubbles is seen. No bubbles at grain boundaries were observed. During the in-situ implantation, the bubble concentration appeared to saturate well before the dose of 2×10^{20} ion m^{-2}. This effect occurred for all the alloys and for pure Zr. A typical bubble size distribution for pure Zr is shown in Fig. 4; some evidence of bubble alignment can also be seen. Although we expected that some of those small bubbles would be solid, no extra electron diffraction spots from solid Kr were found and therefore the question could not be resolved.

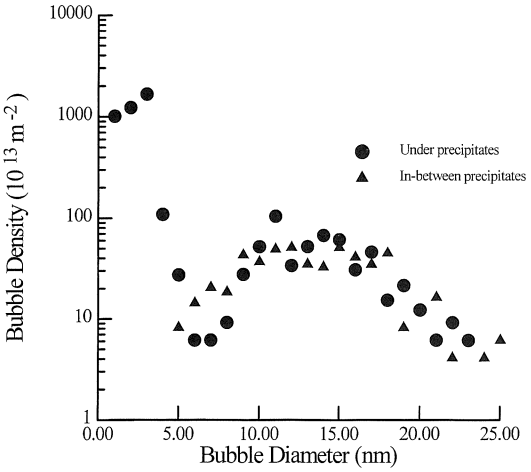

Fig. 10. Bubble size distribution in Zircaloy-4 after irradiation with 100 keV Kr ions to 2×10^{20} ion m^{-2}, at 800°C. Two histograms are shown, one for under the precipitates, one for in-between. The zone under the precipitates has a high density of small bubbles.

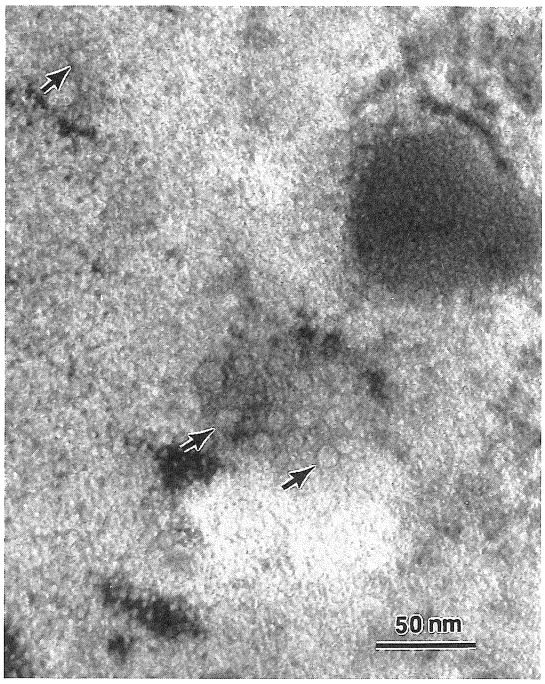

Fig. 11. Bright field contrast in underfocus conditions of Valloy, irradiated with Kr ions to 2×10^{20} ion m^{-2}, at 300°C, under thin foil conditions. Clusters of medium size bubbles (approximately 10–12 nm) are seen in the arrowed regions.

Bulk Zircaloy-4, implanted to a dose of 2×10^{20} ion m^{-2}, exhibits a markedly different type of behavior, Fig. 5a. The bubble distribution after implantation at 300°C was similar to that found in a 'thin foil' irradiation, but implanting at 500 and 700°C resulted in much larger faceted bubbles Fig. 5b. At 500°C even small bubbles were faceted, indicating good atomic surface mobility. The bubble sizes at 700°C (Fig. 5c) were quite large and bubble coalescence was observed. At 700°C a higher concentration of bubbles near grain boundaries was also seen (Fig. 6). Bubbles at the grain boundaries are no longer faceted and are approximately twice as big as the bubbles within the grain.

A TEM image of bulk Zircaloy-4 implanted to a dose of 2×10^{20} ion m^{-2} at 800°C is shown in Fig. 7. Evidence of a significant amount of bubble coalescence is seen in Fig. 7, as well as bubble faceting and some bubble agglomeration at grain boundaries (not shown) where they grew to slightly bigger sizes. After this irradiation at 800°C, we observed plate-like precipitates, shown in low magnification bright-field in Fig. 8, and in dark-field in Fig. 9. These are likely hydrides or oxides, which formed on the specimen free surface during this irradiation. We believe this to be an artifact, possibly related to vacuum conditions at the time of the experiment. Compositional

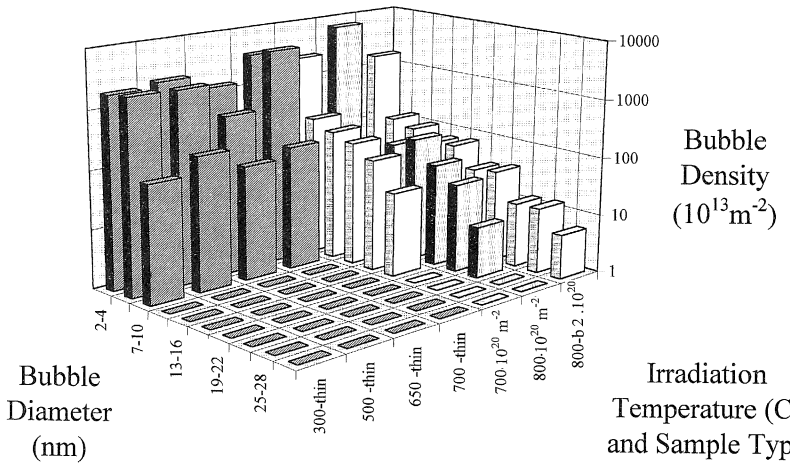

Fig. 12. Bubble size distribution for thin foil and bulk Zircaloy-4 at several temperatures. Thin foil irradiations are indicated.

analysis of the precipitates by EDX revealed that they were not enriched in any of the Zircaloy-4 alloying elements (Sn, Fe, Cr, Ni), and that there was only a slight increase in the Kr concentration. Diffraction patterns from the precipitate were not identified. Interestingly, the Kr bubble distribution was different under (or in) the precipitates than in-between precipitates. The bubble size distributions for both 'under' and 'between' precipitates is shown in Fig. 10. The distribution of large-size bubbles was the same, but the region under the precipitates contained a large density of small (6 nm) bubbles (region marked 'A' in Fig. 7), which was absent between precipitates (region marked 'B' in Fig. 7). It is possible that the precipitates made it more difficult for the gas to leave the thin foil.

There was little effect of alloy type on the bubble size distributions for 'thin foil' experiments from 300–700°C. The only exception was Valloy where some larger bubbles (10–13 nm) were seen in clusters (Fig. 11). It should also be mentioned that the usual intermetallic precipitates found in Zircaloy were seen in these samples (about 0.1 μm in size, distributed unevenly through the solid). Some of these were followed during irradiation and no preferential role in bubble nucleation, trapping or growth was observed for the in-situ irradiations (where bubbles formed were small). For the bulk irradiated samples, the type of homogeneous distribution of bubbles observed in Fig. 7 does not indicate that the intermetallic precipitates normally found in Zircaloy (not to be confused with the 'artifact' precipi-

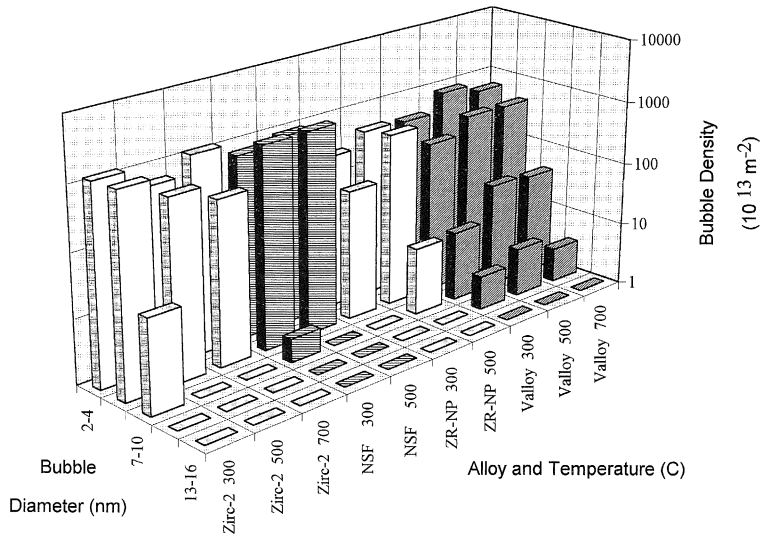

Fig. 13. Bubble size distribution in thin foil of various alloys irradiated at temperatures ranging from 300 to 700°C. Irradiation was conducted to 10^{20} ion m^{-2}.

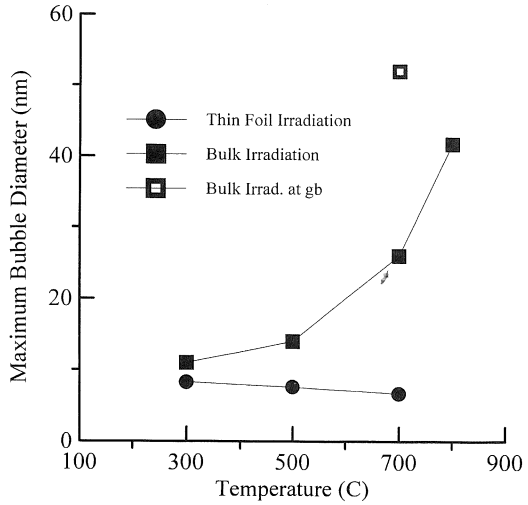

Fig. 14. Maximum bubble diameter in Zircaloy-4 after Kr ion irradiation to 2×10^{20} ion m^{-2} at temperatures ranging from 300 to 700°C.

tates shown in Figs. 8 and 9) had any role in the bubble growth process.

A summary of bubble size distributions is shown in Figs. 12 and 13. The difference between 'thin foil' and 'bulk' irradiation is clearly seen, as is the effect of Kr fluence. Fig. 12 shows the change in bubble size distribution for Zircaloy-4 as a function of irradiation conditions at temperatures ranging from 300 to 800°C (bulk irradiations at 300 and 500°C are not plotted in this graph). The extension of the bubble distribution to larger sizes in bulk specimens at 700 and 800°C is clearly visible. The thin foil irradiations by contrast produce only small bubbles. Fig. 13 shows the bubble size distribution from thin foil irradiations of the different alloys. With the exception of Valloy, which shows a small number of bubbles with diameters in the 10–12 nm range, the bubbles in these samples were all in the 3–8 nm range, regardless of the irradiation temperature within the range 300–700°C.

Fig. 14 shows the maximum bubble size against irradiation temperature for 'thin foil' and 'bulk' specimens of Zircaloy-4. These were obtained by examining several prints at different tilts to identify the largest bubble diameter for each temperature. The peak diameter is relatively independent of temperature for thin foil specimens while it increases markedly with temperature for the bulk specimens. These results are discussed in the next section.

4. Discussion

The growth of voids in solids depends on the agglomeration of irradiation-created vacancies into three-dimensional cavities, as occurs in metals that undergo void swelling. In the absence of gas, irradiation of Zr and Zr alloys does not produce this result, but rather produces vacancy loops which are two-dimensional vacancy aggregates. It is only in the presence of noble gases that three-dimensional cavities are stabilized; hence both vacancies and gas atoms need to come together to produce cavities, which then should properly be called bubbles. Thus, for these bubbles to grow a constant supply of vacancies and gas atoms is needed if the bubbles themselves are immobile. In this scenario both vacancies and gas atoms need to be mobile at the irradiation temperature to effect bubble growth. Bubble growth by this mechanism would produce an homogeneous bubble size distribution. Another possibility is that the bubbles themselves are mobile and grow by coalescence. In that case, when the bubbles are very small, they could be immobile because they are solid bubbles [18]; as they grow they would melt and become mobile and finally reach a size where they again become immobile. This process would produce a bimodal size distribution of bubbles.

In the present experiments, vacancy supply from irradiation is plentiful, and hence bubble growth is controlled by gas arrival at the bubbles, that is, by Kr atom diffusion in the zirconium (alloy) matrix. The temperature at which the maximum bubble size is observed is much higher than previous reports of cavity growth in zirconium alloys. Faulkner and Woo observed maximum void swelling under neutron irradiation at 450°C (after pre-injection with He), whereas in the present work the cavities at 800°C were clearly bigger than those at 500°C. If bubble growth depends on gas mobility, this difference is likely due to the lower migration temperature for He atoms than Kr atoms. It is reasonable that the temperature at which He atoms are mobile is lower than the temperature for Kr atom mobility, which could account for the different temperature regimes for bubble growth.

The results of Buckley and Manthorpe also show a peak in swelling between 400–500°C during electron irradiation of thin specimens of pure Zr (in this case doped with Xe). These results are more difficult to explain in terms of the picture above, since Xe atoms are likely to be mobile in zirconium at higher, not lower, temperatures than Kr. However, as mentioned previously, the vacuum conditions in these experiments were not ideal, which could have played a role in the evolution of these samples under irradiation.

An additional difference in our work from that of Faulkner and Woo [13] is that they found He-stabilized voids (or low-pressure bubbles) during irradiation of thin foils, while we did not. The difference is likely due to their pre-implantation of 100 ppm He as a void stabilizer during electron irradiation, while we used Kr to both stabilize the cavities and to produce displacement damage. Another factor that could explain the difference could be Kr bubbles become mobile and coalesce at a higher temperature than voids or dilute He bubbles.

We attempted to account for the implanted Kr through

use of Ronchi's equation of state for rare-gas bubbles in solids [25], assuming that the bubbles were at equilibrium cavity pressures. Equilibrium bubbles are those which obey the equation:

$$p + \sigma = \frac{2\gamma}{r} \tag{1}$$

where p is the internal gas pressure, σ is the applied stress in the solid, γ is the surface tension and r is the bubble radius. Although the assumption of equilibrium is reasonable [18], we have no direct evidence that the bubbles are in fact in equilibrium, so the following calculation of gas content should be regarded as a rough estimate. Ronchi's equation is given by:

$$p\frac{V}{NRT} = F(r) \tag{2}$$

where p is the bubble pressure, V is the volume, T is the temperature, N is the number of gas atoms, R is the gas constant and r is the radius. The function $F(r)$ is calculated and presented in tabular form in Ref. [25]. Using the bubble distributions shown in Figs. 10 and 12–14, we calculated the total number of gas atoms in each size category from Eq. (2), assuming equilibrium bubbles. The amount of Kr retained in bulk specimens is approximately 70% while in thin foils it less than 5%. This supports the theory that the difference between the thin foil and bulk cases is due to Kr gas (either in the form of bubbles or atomic Kr), escaping through the surfaces during thin foil implantation. The different temperature regimes can be summarized as follows:

Low temperature: Bubbles are immobile and at high pressures, possibly close to that required to solidify the Kr. Bubble growth is gas-driven, controlled by the steady state gas concentration and gas flux to the bubbles. Bubbles reach a steady state size distribution centered around 3 nm diameter bubbles. The reason for the steady state could be an equilibrium between gas and vacancy injection and loss of material from the bubbles by recoil dissolution.

High temperature: At higher temperatures, very small bubbles are immobile, either because they are solid or because of high pressure [27]. As bubble size increases, the pressure decreases and at a critical bubble radius they become mobile (possibly associated with Kr melting). When bubbles become mobile, they can coalesce with other bubbles or leave the specimen through a nearby surface. Mobile bubbles in thin specimens are much more likely to reach a free surface than those migrating in bulk material, where they have some probability of moving away from the free surface. Thus bubble coalescence is much more likely in bulk specimens than in thin foils. As the bubbles grow, their mobility decreases [26]: depending on the atomic transport mechanism, the bubble diffusion coefficient is proportional to $1/r^n$, with $n = 2$, 3 or 4, and where r is the bubble radius. Regardless of the model for bubble migration, if the bubble mean free path and lifetime are long enough, a bubble will grow to a point when it is effectively immobilized. This will result in a much higher proportion of the implanted gas being retained in bulk specimens.

Part of the difference between thin foil and bulk irradiation may be attributed to Kr and possibly vacancy loss to free surfaces. This interpretation is supported by enhanced small bubble retention in the presence of the 'plate-like' surface precipitates shown in Fig. 8. When the precipitates were present, the Kr loss to the foil surface was suppressed, thereby increasing the total amount condensed into bubbles. Similar results were attained for thin specimens implanted in both the HVEM and in the ion chamber indicating that the suppression of large bubbles in thin specimens is not related to the vacuum conditions, dosimetry or temperature control.

According to our model, the temperature at which the peak bubble size occurs is the temperature at which Kr bubbles become mobile and coalesce. This occurs at a much higher temperature than the previously reported peak swelling during neutron and electron irradiation of Zr [10,12,13]. This is likely an indication of the different nature of the two processes: void swelling being controlled by vacancy migration, and the gas swelling determined by gas and bubble migration. If void swelling occurs by a mechanism of He-assisted nucleation followed by void growth from vacancy absorption, then the activation energy could correspond to vacancy migration. If the formation of large bubbles is controlled by bubble coalescence, it would not be surprising that it occurs at a different temperature. If the temperature dependence of bubble size is related to gas migration, it is also not surprising that different gases have different peak bubble size temperatures.

A surprising result of this work is that there is little difference in bubble sizes in the different materials implanted. In particular, there was no difference between nominally pure Zr and the Zr alloys. Since alloying elements have been shown to influence defect diffusion [5], and void formation [12], this result was unexpected. This absence of effect may be due to the use of thin specimens. The presence of the nearby surface sinks in these experiments may have overwhelmed all other processes, thereby masking any possible differences in migration between the different alloys.

5. Conclusions

A systematic study was conducted of bubble formation in Zircaloy-4 and other Zr alloys under Kr ion irradiation. The main conclusions of this study are:

(1) Bubbles form in all alloys, at all temperatures and implantation geometries studied. This is in agreement with previous results that show that cavity formation in Zr

alloys under irradiation is greatly enhanced by the presence of noble gases.

(2) The bubble sizes observed in bulk samples were considerably larger than in thin samples. This is attributed to the greater loss of both gas atoms and vacancies to the surface in the thin foil case.

(3) In the bulk Zircaloy-4 samples, bubble size increased with irradiation temperature. The maximum bubble diameter within the grains increased from 10 nm at 300°C to 40 nm at 800°C. Above 700°C large faceted bubbles and bubble coalescence were found.

(4) For the thin specimens, bubble size did not depend on implantation temperature, in the temperature range 300–700°C. The bubble morphology was similar to that observed in bulk specimens implanted at 300°C, and corresponded to a low temperature gas-driven regime.

(5) The gas retained in the samples after irradiation, calculated using Ronchi's equation of state and assuming equilibrium bubble pressures, was much higher in bulk samples than in pre-thinned foils.

Acknowledgements

The authors would like to thank Ed Ryan, Loren Funk, Peter Baldo, and Stan Ockers of the HVEM/Tandem Facility in the Center for Electron Microscopy at Argonne National Laboratory (ANL) for their expert technical assistance in performing the irradiations. The assistance of Bernie Kestel, also of ANL in TEM sample preparation is greatly appreciated. We thank Ron Adamson of General Electric, Vallecitos, for furnishing the Zr alloys for this study. We acknowledge helpful discussions with L.M. Howe. L. Pagano, Jr. was supported by the Brazilian Government while pursuing his thesis research.

References

[1] C. Lemaignan and A.T. Motta, in: Materials Science and Technology, Nuclear Materials, ed. B.R.T. Frost, Vol. 10, part B (VCH, 1994) pp. 1–51.
[2] D. Faulkner and M.P. Puls, Proc. Int. Conf. on Fundamental Aspects of Radiation Damage in Metals, Gatlingburg, TN (1975) CONF-751006-P2, pp. 1287–1295.
[3] C.D. Williams and R.W. Gilbert, Radiation Damage in Metals, Vol. 1 (IAEA, Vienna, 1969) p. 235; D.O. Northwood and R.W. Gilbert, Radiat. Eff. 22 (1974) 139–140.
[4] A. Wolfenden and K. Farrell, Scr. Metall. 6 (1972) 127–130; 7 (1973) 39–42.
[5] G.M. Hood, H. Zou, R.J. Schultz, J.A. Roy and J.A. Jackman, J. Nucl. Mater. 189 (1992) 226–230.
[6] Y. Adda, Proc. Conf. on Radiation Induced Voids in Metals, Albany, 1971, eds. J.W. Corbett and L.C. Ianniello, USAEC Symp. Ser. No. 26 (1972) pp. 338–362.
[7] D.I.R. Norris, Radiat. Eff. 14 (1972) 1–37.
[8] G.J.C. Carpenter, Radiat. Eff. 11 (1973) 189–190.
[9] R.W. Gilbert, K. Farrell and C.E. Coleman, J. Nucl. Mater. 84 (1979) 137–148.
[10] A. Jostsons, P.M. Kelly, R.G. Blake and K. Farrell, ASTM STP 683, eds. J.A. Sprague and D. Kramer (1979) pp. 46–61.
[11] M. Griffiths, R.W. Gilbert and C.E. Coleman, J. Nucl. Mater. 159 (1988) 405–416.
[12] S.N. Buckley and S.A. Manthorpe, Proc. Conf. on Physical Metallurgy of Reactor Fuel Elements, Berkeley, UK, 1973, pp. 127–131.
[13] D. Faulkner and C.H. Woo, J. Nucl. Mater. 90 (1980) 307–316.
[14] M. Griffiths, R.C. Styles, C.H. Woo, F. Phillip and W. Frank, J. Nucl. Mater. 208 (1994) 324–334.
[15] S.E. Donnelly and J.H. Evans, eds., NATO Advanced Research Workshop on Fundamental Aspects of Inert Gases in Solids, Vol. 279 of NATO Advanced Study Institute, Series B: Physics (Bonas, France, 1990).
[16] R.C. Birtcher and W. Jager, Ultramicroscopy 22 (1987) 267–280.
[17] S.E. Donnelly and C.J. Rossouw, Nucl. Instrum. Methods Phys. Res. B 13 (1986) 485–489.
[18] R.C. Birtcher and A.S. Liu, J. Nucl. Mater. 165 (1989) 101–109.
[19] J.H. Evans and D.J. Mazey, J. Phys. F: Met. Phys. 15 (1985) L1–L6.
[20] J.H. Evans and D.J. Mazey, J. Nucl. Mater. 138 (1986) 176–184.
[21] J.H. Evans and D.J. Mazey, Scr. Metall. 19 (1985) 621–623.
[22] D.J. Mazey and J.H. Evans, J. Nucl. Mater. 138 (1986) 16–18.
[23] B. Kestel, Ultramicroscopy 19 (9186) 205.
[24] J.F. Ziegler, J.P. Biersack and U. Littmark, The Stopping and Range of Ions in Solids (Pergamon Press, New York, 1985).
[25] C. Ronchi, J. Nucl. Mater. 96 (1981) 314–328.
[26] D. Kaletta, Radiat. Eff. 78 (1983) 245–259.
[27] J. Rest and R.C. Birtcher, J. Nucl. Mater. 168 (1989) 312.